L. Cortelezzi, S. Ferrari, G. Dubini
A Scalable Active Micro-Mixer for Biomedical Applications
Microfluidics and Nanofluidics, Vol. 21, N. 3, 2017, 31 (16 pages)
doi:10.1007/s10404-017-1868-9

Noname manuscript No.
(will be inserted by the editor)

A scalable active micro-mixer for biomedical applications

Luca Cortelezzi[1,2] · **Simone Ferrari**[1] · **Gabriele Dubini**[1,3]

Received: date / Accepted: date

Abstract We present a geometrically scalable active micro-mixer suitable for biomedical and bioengineering applications and potentially assimilable in a Lab-on-Chip. Our micro-mixer is able to process volumes of fluid in the range of $10^{-6} \div 10^{-9}$ liters; its actuation system induces fast mixing; its constructive simplicity facilitates its realizability, assimilability and reusability; it is geometrically scalable and, therefore, assimilable to microfluidic systems of different dimensions. We characterize the mixing performance of our micro-mixer in terms of Reynolds, Strouhal and Péclet numbers in order to establish a practical range of operating conditions for our micro-mixer. Finally, we demonstrate the geometrical scalability of our micro-mixer.

Keywords · Microfluidic Mixing · Active Micro-mixer · Scalable Micro-mixer

1 Introduction

One of the main targets of microfluidics is to assemble all functions of a laboratory for chemical/biological analysis on a platform of a few square centimeters in size, in order to create a so called Lab-on-Chip (LoC) [1]. Intrinsic characteristics of microfluidics such as manipulating small volumes ($10^{-6} \div 10^{-9}$ liters) of fluids, producing high speed reactions while requiring low energy consumption, easy transportability and low costs (when compared to the costs of the currently available analysis stations) are attractive benefits for the development and realization of LoC systems. However, the creation of LoC devices for practical applications currently encounters the difficult problem of assimilating large number of microfluidic components over a single, fully automated platform, easily usable [2]. This problem has not been overcome as yet, and, at the moment, most of the microfluidic systems, successfully tested in laboratories, are chip-in-a-lab, instead of lab-on-a-chip, and have only limited functionality [3].

Micro-mixers are essential components of LoC systems because mixing is a fundamental process in many chemical and biological microfluidic applications. Chemical applications include crystallization [4], extraction [5], polymerization [6] and organic synthesis [7–9], to name a few, while biological applications include enzyme assays [10], biological screening, such as selective sorting of biomolecules [11–13] or cells [14], bioanalytical processes, such as cell separation [15], cell lysis [16, 17], DNA analysis [18] and μTAS [19], and protein folding [20,21], to name a few. Therefore, it is extremely useful to design and test compact, efficient, fast, geometrically scalable and easily assemblable micro-mixers, which is the goal of the present article.

Micro-mixers are generally classified in two main categories: passive or active [22]. In general, passive micro-mixers rely entirely on molecular diffusion to induce mixing in long thin channels or networks of channels, whose geometry is specifically designed to increase the surface of the interface separating the fluids to be mixed. To reduce the dimensions of passive micro-mixers,

Corresponding author: Luca Cortelezzi
E-mail: luca.cortelezzi@polimi.it

[1]Laboratory of Biological Structure Mechanics, Politecnico di Milano, Italy

[2]Department of Aerospace Sciences and Technologies, Politecnico di Milano, Italy

[3]Dipartimento di Chimica, Materiali ed Ingegneria Chimica "G. Natta", Politecnico di Milano, Italy

different designs have been proposed in literature, for example serpentines [23], spirals [24] and split and recombination micro-mixers [25]. To accelerate the mixing process, new types of passive micro-mixers able to generate chaotic advection [26] have been proposed by several authors: Johnson *et al.* (2002) [27], Stroock *et al.* (2002) [28], Ottino and Wiggins (2004) [29], Kim *et al.* (2004) [30], Garofalo *et al.* [31]. to name a few. On the other hand, active micro-mixers, in general, substantially enhance mixing by actively promoting stretching and folding of the mixture through the action of appropriate actuators that intelligently modify the time evolution of the hydrodynamic field. Active micro-mixers can be classified in accord to the type of external field induced/leveraged by the actuators: pressure [32], temperature [34], electrohydrodynamic [35], dielectrophoretic [36], electrokinetic [37], magnetohydrodinamic [38] and acoustic [39], to name a few. Thanks to their simple design and easy assimilability in microfluidic systems, passive micro-mixers have been often preferred over the more sophisticated active micro-mixers. However, the latter are more compact and have a substantially better mixing performance.

This article presents a geometrically scalable active micro-mixer suitable for a wide range of biomedical/bioengineering applications and potentially assimilable in a LoC. Our goal is to design a micro-mixer, having a simple geometry and robust performance, able to induce fast mixing over a wide range of operating conditions. In other words, our goal is to design a workhorse micro-mixer, robust and reliable, that could be further optimized to meet the requirements of different biomedical/bioengineering applications. We conceived our micro-mixer with the intent of satisfying the following constraints: small dimensions, because the device must be able to process volumes of fluid in the range of $10^{-6} \div 10^{-9}$ liters; high mixing speed, because mixing should be obtained in the shortest possible time; constructive simplicity, to facilitate realizability, assimilability and reusability of the micro-mixer; and geometrical scalability, because the micro-mixer should be assimilable to microfluidic systems of different dimensions. Note that we are not specifying any quantitative design requirement for the mixing time because it depends on a combination of the size of the micro-mixer, the frequency of forcing and the properties of the fluids to be mixed and, therefore, the mixing time changes with the geometric dimensions of the micro-mixer. Our target is to achieve complete mixing in the shortest time by keeping the geometry as compact as possible and the actuation system as efficient as possible.

In conceiving our active micro-mixer, we focused on two crucial aspects: the geometry of the device and the actuation system. The former is important for the practical realizability and assemblability of the device, and the latter, in particular, should be designed to favor the implementability of the device in a LoC. The geometry of our micro-mixer takes inspiration from the work of Cubaud and Mason (2009) [40], who realized a diverging-converging micro-channel to study experimentally the interactions between two liquids having a very high (up to 500 times) viscosity differential. The authors showed that this geometry favors the onset of surface tension instabilities at the interface between the two fluids inducing their mixing. In our case, however, we are targeting biomedical applications where the two fluids to be mixed have similar properties, close to the properties of water, i.e. aqueous solutions. For these types of fluids, the geometrical/operational configuration proposed by Cubaud and Mason (2009) [40] does not favor mixing, as it will be shown later, because no instabilities can be induced. Therefore, we modified and transformed the passive mixer proposed by Cubaud and Mason (2009) [40] into an active mixer by forcing harmonically in time the flow in the lateral channels [32, 41–43], see figure 1.

Fluid flows in microfluidic devices are, in general, strictly laminar and, therefore, dominated by viscous effects. Mixing in laminar regimes is hard to achieve and efforts have been made over the years to overcome this difficulty. The study of laminar mixing began with the pioneering work by Aref (1984) [26], who introduced the concept of chaotic advection, and stimulated numerous studies on laminar mixing, for example Ottino 1989 [44]; Aref & El Naschie 1995 [45]; Alvarez et al. 1998 [46]; Zalc & Muzzio 1999 [47]; Aref 2002 [48]; Szalai et al. 2003 [49]; Gleeson 2005 [50]; Gouillart, Thiffeault & Finn 2006 [51]; Phelps & Tucker 2006 [52]; Sturman, Ottino & Wiggins 2006 [53]; Vikhansky & Cox 2007 [54], Cortelezzi & Mezić [55], to name a few. It has been shown that the quality of mixing strongly depends on two main factors: the geometry of the initial concentration field (e.g., [56]) and, for a given actuation system, the time sequence of the actuations used to stir the mixture (e.g., [57]). Note that a given actuation strategy will perform differently depending on the initial geometry of the concentration field. More importantly, with a poorly chosen actuation system, fluid homogenization can be achieved mainly by molecular diffusion.

Glasgow and Aubry (2003) [32] investigated mixing enhancement in a T-shaped micro-channel where the flow in one or both inlets (located at the tip of the arms of the T) was forced periodically. They showed that the best mixing performance was achieved by pulsing, out-of-phase in time, the flows at both inlets. Subsequently,

Glasgow, Lieber and Aubry (2004) [33], characterized, for the same T-shaped micro-mixer, the dependency of the mixing performance on some dimensionless parameters (e.g., Strouhal number). They showed that higher Strouhal numbers (ratio of the flow characteristic time to the period of pulsation) and pulsed volume ratios (ratio of the volume of fluid pulsed to the volume of inlet/outlet intersection) led to better mixing. Muller *et al.* (2004) [41] proposed an evolutionary optimization of an active micro-mixer composed by a main channel orthogonally intersected by three pairs of secondary channels. The fluids to be mixed are both injected through the main channel, while through the secondary channels are applied oscillating zero-mean flow rates, with specific frequencies and phase shifts, in order to perturb intelligently the flow in the main channel and promote mixing. The authors showed that mixing was substantially enhanced when forcing of increasing frequencies was applied through the three pairs of transverse channels. Sun and Sie (2010) [43] considered a micro-mixer composed by a T-shaped entrance channel, a diverging section, and a wide exit channel. At the two inlets (located at the tip of the arms of the T) were applied periodic pressure fields and the geometry of the diverging section was modified by changing its half-angle. The mixing performance was characterized in terms of the half-angle of the diverging section and the phase difference between the actuating pressure fields. The authors showed that an appropriate diverging micro-channel greatly improves mixing, compared to a straight micro-channel, because, on the one hand, it favors stretching and folding of the lamellae generated by the pulsating pressure fields, while, on the other hand, it decelerates the flow allowing more time to molecular diffusion to further homogenize the mixture. In this study we combine some of the above ideas with some of the ideas and results on mixing optimization presented by Gubanov and Cortelezzi [58,59].

Figure 1 shows the geometry of our micro-mixer. The two fluids to be mixed are injected through the three micro-channels on the left. In the central micro-channel is injected a medication (e.g., dopamine, strontium ranelate, etc.) at a constant flow rate, while through the lateral micro-channels is injected the carrier, or parenteral, solution (e.g., distilled water) at time-dependent out-of-phase flow rates. The streams of medication and carrier solution merge and interact at entrance of the mixing micro-chamber creating a sequence of lamellae of opposite concentration. The circular mixing chamber acts as a diffuser, it decelerates the flow and favors the stretching of the lamellae, while the cylindrical obstacle splits the incoming flow and enhance folding of the lamellae. Finally, the mixture outflows through the exit micro-channel on the right favoring further stretching of the lamellae. Note that there is little hope to study analytically the performance of our micro-mixer because of its geometry, although simple is still too complex, and its active actuation system. To the best of our knowledge, only passive, linear micro-mixers with very simple geometries, typically, T and Y shaped micro-mixers have been analyzed analytically and/or experimentally, see, for example, Ismagilov *et al.* (2000) [60] and Nguyen & Wu (2005) [22]. Therefore, we decided to adopt a Computational Fluid Dynamics (CFD) approach to design an active, scalable micro-mixer and characterize its mixing performance.

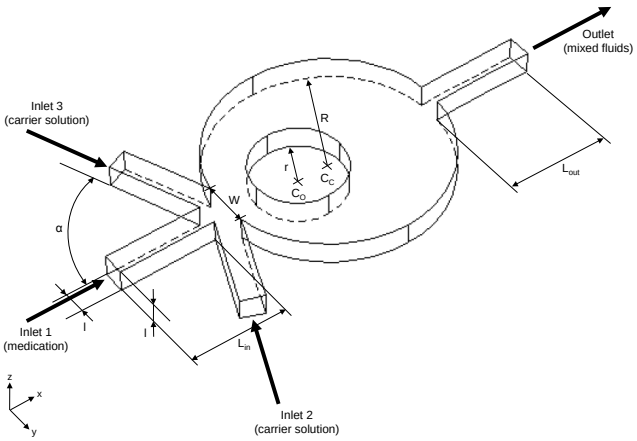

Fig. 1 Geometry of the scalable active micro-mixer.

This article characterizes numerically the mixing performance of our micro-mixer (see figure 1) in terms of Reynolds, Strouhal and Péclet numbers in order to establish a practical range of operating conditions for our micro-mixer. It shows that our micro-mixer satisfies the design and operational requirements we discussed above. Its geometry is extremely simple involving four micro-channels (three inlets and one outlet) of the same size, a cylindrical mixing chamber and a cylindrical obstacle, all elements that can be easily micro-manufactured. Its constructive simplicity facilitates its realizability, assimilability and reusability. The actuating system needed to create the oscillatory flows in the lateral micro-channels can be implemented by using, depending on the geometric dimensions of the micro-mixer and the frequency of forcing, programmable syringe pumps or pressure-based flow controllers or piezoelectric micro-pumps. Being active our micro-mixer is more compact than the passive ones and induces mixing at a faster rate than passive micro-mixers. Furthermore, our micro-mixer is geometrically scalable and, there-

fore, able to process volumes of fluids in the range of $10^{-6} \div 10^{-9}$ liters and it is assimilable to LoC systems of different dimensions.

This article is organized as follows: In section 2, we present the mathematical formulation and provide details about the numerical simulation of the flow within the micro-mixer. In section 3, we present and discuss the results of our two- and three-dimensional simulations in terms of Reynolds, Strouhal and Péclet numbers. Furthermore, we discuss the geometrical scalability of our device. In section 4, we summarize our study and present our conclusions.

2 Mathematical modeling and numerical simulation

Figure 1 shows the geometry of our micro-mixer. The two fluids to be mixed are injected through three identical micro-channels having a square section of side l. Through the central micro-channel is injected the medication/pharmacological fluid (e.g., dopamine, strontium ranelate, etc.) at constant flow rate Q_M, while through the two lateral micro-channels (which are oriented at an angle α with respect to the central micro-channel) is injected the carrier solution (e.g., distilled water) by superposing a mean flow rate $Q_C = Q_M/2$ to a harmonically oscillating flow rate Q_O. Note that the flows in the two lateral micro-channels oscillate in opposition of phase. The steady flow through the central micro-channel merges with the time-dependent flows incoming from the lateral micro-channels. As these streams enter a cylindrical mixing micro-chamber of radius R, through an opening of width W, they interact and create a sequence of thin lamellae of opposite concentration. The circular mixing micro-chamber acts as a diffuser, it decelerates the flow and favors the stretching of the lamellae. A cylindrical obstacle of radius r, centered at a distance d from the center of the chamber, splits the incoming flow in two streams and induce the folding of the lamellae. Furthermore, this obstacle reduces the volume of the mixing micro-chamber and, therefore, decreases the transient-time needed by the micro-mixer to reach its regime operating conditions. Finally, the mixture exits through a micro-channel of square section of side l, identical to the inlet micro-channels. Note that the angle α, the width W, the radius r and location $d = C_c - C_o$ of the obstacle have been chosen through a coarse optimization. For each parameter (α, W, r and d), we defined an admissible range and tested, within this range, three different values and choose the value of the parameter that produced the best mixing performance. A more refined optimization is, of course, possible, but it is above the scope of this article that presents a simple and robust design of a reliable and versatile micro-mixer. It is left to the final user of the micro-mixer to perform, if needed, further optimizations once the final application, geometric dimensions and physical properties of the fluids involved are known.

In this study we are targeting biomedical applications where the two fluids to be mixed have similar properties. Therefore, the two fluids are both modeled as incompressible and viscous having physical properties similar to water (i.e. density $\rho = 1000 kg/m^3$, viscosity $\mu = 0.001 Pa \cdot s$, molecular diffusivity $D = 10^{-10} m^2/s$) with the only difference being the value of the passive scalar (e.g., concentration of a tracer, temperature, etc.) they transport. The time-evolution of the two fluids is governed by continuity and momentum equations, while the time-evolution of the concentration field is governed by the advection-diffusion equation. Note that we assume that the scalar is passive or, in the case of an active scalar, that the gradients of the concentration field are small enough so that the mathematical problem is one-way coupled, i.e. the time-evolution of the hydrodynamic field governs the evolution of the scalar field, while the evolution of the scalar field does not affect the evolution of the hydrodynamic field.

2.1 Mathematical formulation

We make the problem dimensionless by defining as characteristic length W, the width of the entrance to the mixing micro-chamber, as characteristic time $T = 1/f$ the inverse of the frequency of forcing f, and as characteristic velocity the magnitude V of the velocity in the central micro-channel. Note that there are three possible characteristic lengths in this problem: the side l of the micro-channels, the radius of the mixing chamber R, and the width W. We choose W as a characteristic length because W controls the level of the interaction between the forced flows incoming from the lateral micro-channels and the steady flow incoming from the central micro-channel. A correct choice of W is crucial for the formation of a sequence of lamellae of opposite concentration. In fact, a width, W, too small limits the effects of forcing to the area where the three micro-channels converge and, as a consequence, the lamellae being generated are small and thick. On the other hand, a width, W, too large allows the outflow of the forcing streams in the mixing chamber almost without interacting with the steady flow, therefore inhibiting the formation of the lamellae.

Using the above characteristic quantities, we make the problem dimensionless. The time-evolution of the

Table 1 Summary of the results of a mesh sensitivity study performed by discretizing the volume of the reference micro-mixer of dimensions $W_r = 200\mu m$, $R = 2.5W_r$, $r = W_r$, $l = 0.5W_r$, $L_{in} = 2W_r$, $L_{out} = 2.25W_r$, $d = C_c - C_o = 0.75W_r$, $\alpha = 67.5°$, with volume flow rates $Q_{Mr} = 10^8 \mu m^3/s$, $Q_{Cr} = Q_{Mr}/2$, $Q_{Or} = 4Q_{Mr} = 8Q_{Cr}$, and frequency of forcing $f_r = 40Hz$ when operating at $Re = 2$, $St = 0.8$ and $Pe = 10^4$.

	2D			**3D**
	Grid #1	Grid #2	Grid #3	
Element size (μm)	10	5	2.5	10
Number of elements	17177	69504	277931	310390
Minimum orthogonal quality (low quality = 0 ÷ 1 = high quality)	0.494992	0.594102	0.509791	0.400012
Maximum ortho skew (low quality = 0 ÷ 1 = high quality)	0.288558	0.263737	0.297942	0.567376
Maximum aspect ratio	4.57155	4.30973	4.62624	9.92841
CPU time (2 Quad-Core Intel®Xeon®E5620 (2.40GHz)) (days)	1.7	6.7	26.7	36.7

hydrodynamic field is governed by the dimensionless Navier-Stokes and continuity equations

$$St\left(\frac{\partial \boldsymbol{v}}{\partial t} + \boldsymbol{v}\cdot\boldsymbol{\nabla}\boldsymbol{v}\right) = -\boldsymbol{\nabla}p + \frac{1}{Re}\boldsymbol{\nabla}^2\boldsymbol{v}, \tag{1}$$

$$\boldsymbol{\nabla}\cdot\boldsymbol{v} = 0, \tag{2}$$

where $\boldsymbol{v} = [u\ v\ w]^*$ is the velocity vector field, p is the pressure, $Re = \rho VW/\mu$ is the Reynolds number, $St = fW/V$ is the Strouhal number, ρ is the density, μ is the dynamic viscosity and $*$ indicates transpose. The no-slip and no-penetration boundary conditions are imposed on the entire internal surface of the micro-mixer. The inflow conditions are as follows: at Inlet 1 (the entrance of the central micro-channel, see figure 1), the magnitude of the velocity is equal to unit, i.e. $|\boldsymbol{v}| = 1$; at Inlet 2 (the entrance of the right side micro-channel, see figure 1) the magnitude of the velocity is $|\boldsymbol{v}| = 0.5 + V_f \sin(2\pi f)$; at the Inlet 3 (the entrance of the left side micro-channel, see figure 1) the magnitude of the velocity is $|\boldsymbol{v}| = 0.5 - V_f \sin(2\pi f)$, i.e. it oscillates in opposition of phase with respect to the velocity at the Inlet 2. Finally, the gauge pressure value is set to be $p = 0$ at the Outlet (see figure 1). The initial condition for the velocity vector field is $\boldsymbol{v} = \boldsymbol{0}$ everywhere inside the micro-mixer.

The time-evolution of the concentration, c, of the passive scalar field is governed by the dimensionless advection-diffusion equation

$$St\left(\frac{\partial c}{\partial t} + \boldsymbol{v}\cdot\boldsymbol{\nabla}c\right) = \frac{1}{Pe}\boldsymbol{\nabla}^2 c, \tag{3}$$

where $Pe = VW/D$ is the Péclet number. Zero-flux boundary condition, i.e. $\boldsymbol{\nabla}c\cdot\boldsymbol{n}$, is imposed on the entire internal surface of the micro-mixer, where $\boldsymbol{n}$ is the inward normal to the internal surface. The inflow conditions are as follows: $c = 1$ at Inlet 1 and $c = 0$ at Inlet 2 and Inlet 3 (see figure 1). The initial condition for the concentration field is $c = 0$ everywhere inside the micro-mixer. In other words, we assume that the micro-mixer is initially entirely filled with carrier solution, a safety procedure adopted in hospitals to avoid injecting a patient with an overdose of medication.

2.2 Numerical simulations

We discretize and solve the governing equations using a Finite Volume Method (FVM) [61]. The computational domain is discretized by means of an unstructured (free) mesh of triangular elements in two-dimensions and tetrahedral elements in three-dimensions, generated by the solid modeler ICEM (Ansys, Canonsburg, PA, USA). In general, the use of a free mesh provides a greater flexibility in discretizing complex domains, at the expense of a lower accuracy than that achievable using a man-developed structured mesh, being, in the former case, the arrangement of the elements entirely determined by a software.

The numerical simulations of the flow within the micro-mixer were performed using the commercial FVM software Ansys Fluent 14 (Ansys, Canonsburg, PA, USA). The time integration was performed using a first-order implicit scheme while the space integration was performed using a second-order upwind scheme. Under the assumption that the scalar field is passive, i.e. it does not affect the time evolution of the velocity and pressure fields, or its gradients are sufficiently small in the case of an active scalar field, the problem is one-way coupled and, therefore, we first solved Navier-Stokes (1) and continuity (2) equations to calculate the time-evolution of the hydrodynamic field and, subsequently, we solved the advection-diffusion equation (3) to obtain the associated time-evolution of the scalar field.

Table 1 summarizes the results of a mesh sensitivity study performed by discretizing the volume of a reference micro-mixer of dimensions $W_r = 200\mu m$, $R = 2.5W_r$, $r = W_r$, $l = 0.5W_r$, $L_{in} = 2W_r$, $L_{out} = 2.25W_r$, $d = C_c - C_o = 0.75W_r$, $\alpha = 67.5°$, with volume flow rates $Q_{Mr} = 10^8 \mu m^3/s$, $Q_{Cr} = Q_{Mr}/2$, $Q_{Or} =$

$4Q_{Mr} = 8Q_{Cr}$, and frequency of forcing $f_r = 40Hz$ when operating at $Re = 2$, $St = 0.8$ and $Pe = 10^4$. The subscript r indicates that these are the dimensions of the reference micro-mixer. The total volume of the reference mixer is of $83.4 \times 10^6 \mu m^3 = 1.0425 \times W_r^3$. As it will be shown in Section 3, the flow within the micro-mixer is symmetric with respect to the mid-plane. Therefore, since the complexities of both the computational domain and the geometry of the concentration field are captured in the mid-plane of the micro-mixer, we performed a mesh sensitivity study using a two-dimensional model of the reference micro-mixer. We considered three possible grids with element size of 10 μm (Grid # 1), 5 μm (Grid #2) and 2.5 μm (Grid #3), respectively. Table 1 presents the details of our mesh sensitivity study. Grid #2 was chosen for the two-dimensional model and used to obtain the results presented in Section 3 because it provided the best compromise between good accuracy and acceptable computational cost. Table 1 also provides information regarding the grid used to perform the three-dimensional computations presented in Section 3. Because of the elevate computational cost, the three-dimensional grid uses elements of the same side length as in Grid #1, this choice reduces the accuracy of the computation but make the computational time acceptable, about 36.7 days for the simulation whose concentration field at time $t = 200$ is shown in figure 3 (h). The time step used for the reference micro-mixer is $3.125 \times 10^{-5} s$. while the time step was appropriately rescaled with the frequency of forcing in all other cases. We considered our simulations well converged when the normalized residuals for the mass, the velocity components and scalar field fell below the value of 10^{-7}. The numerical simulations were performed on one node of a cluster Dell PowerEdge Blade M1000e, where each node is equipped with 2 Quad-Core Intel®Xeon®E5620 (2.40GHz) processors, 24 GB of RAM and 2x146Gb SAS disk storage.

2.3 Quantification of mixing performance

In order to quantify the mixing performance of our micro-mixer, we define a measure of mixing as [43] follows

$$M = 100 \times \left\{ 1 - \frac{1}{Tot} \sum_{j=1}^{Tot} \sqrt{\frac{1}{P} \sum_{i=1}^{P} \left(\frac{c_{ij} - c_{tg}}{c_{tg}} \right)^2} \right\}, \quad (4)$$

where c_{ij} is the value of the concentration of the scalar field measured at the sampling point i (in general not a grid point) at time j, c_{tg} is the target, or desired, value of the concentration, P is the total number of sampling points, evenly distributed over a specified cross-section located at a distance l from the outlet of the exit micro-channel, and Tot is the total number of consecutive instants of time over which a time-average is computed, in this study over one cycle of forcing. Time-averaging over a period of forcing is useful when the values of the concentration field fluctuates with time due to forcing. Note that the P sampling points in general do not coincide with the grid points of the unstructured mesh. Therefore, the value of the concentration field at a given sampling point is obtained by linearly interpolating the known values of the concentration at the adjacent computational grid points. Note that a value of $M = 100\%$ indicates completely mixed fluids, while a value of $M = 0\%$ indicates completely segregated fluids.

3 Results

We verified the absence of any substantial mixing when the medication (white fluid, $c = 1$) and carrier solution (black fluid, $c = 0$) are injected at constant flow rates through the central and lateral micro-channels, respectively. Figures 2 shows the two- and three-dimensional concentration fields for the case $Re = 2$ and $Pe = 10^4$ at time $t = 200$. Note that the two-dimensional model (figure 2 (a)) accurately reproduces the flow in the mid-plane, effectively the symmetry plane, of the three-dimensional micro-mixer (figure 2 (b)). The medication encounters the carrier solution at the intersection of the three inlet micro-channels. The two fluids do not mix as they enter and fill the mixing micro-chamber, and leave it through the exit micro-channel with the medication simply surrounded by the carrier solution. Due to the low molecular diffusion considered ($Pe = 10^4$), a strong concentration gradient is maintained at the interface between the two fluids, from the intersection of the inlet micro-channels, where they encounter initially, to the outlet section, where they leave the device (see figure 2). Note that the presence or not (not shown) of a cylindrical obstacle inside the micro-chamber does not improve mixing under these flow conditions.

In order to induce mixing we force harmonically in time but in opposition of phase the flow in the lateral micro-channels [32,41,43]. Figures 3 (a)-(g) show the time-evolution of the concentration of the scalar field inside the two-dimensional model when $Re = 2$, $St = 0.8$ and $Pe = 10^4$. The comparison between figures 3 (g) and 3 (h) shows that the two-dimensional model reproduces accurately the flow in the symmetry plane of the three-dimensional micro-mixer. The white color represents the concentration of the pure medication ($c = 1$), the black color that of the pure carrier

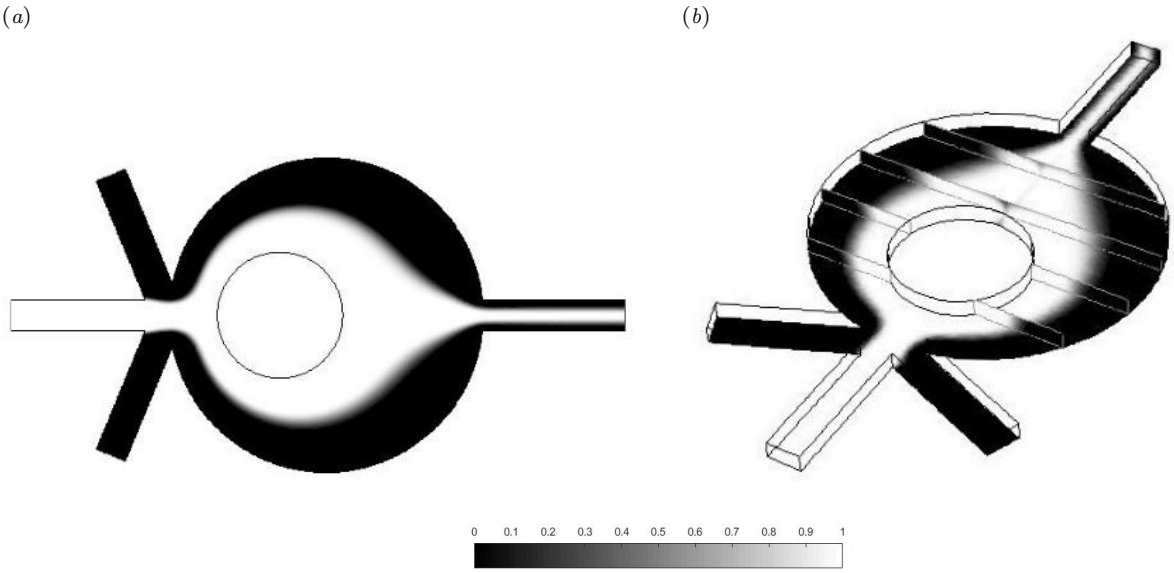

Fig. 2 Concentration of the scalar field in two- (a) and three-dimensions (b) when steady volume flow rate conditions are applied at the three inlets.

solution ($c = 0$) and the different shades of gray (distributed over a linear scale) indicate the different levels of dilution of the medication. Note that initially the micro-mixer is entirely filled with the carrier solution. This is a typical safety procedure (for example in hospitals) to avoid to inject a patient with an overdose of medication. The time-dependent flow of the carrier solution incoming from a lateral micro-channel induces, at every half-period of forcing, a fraction of the medication to flow into the opposite lateral micro-channel where the carrier solution is receding. The remaining fraction of medication flows together with the outflow of carrier solution into the mixing micro-chamber where they form two lamellae of opposite (with respect to a perfectly mixed state) concentration. Figure 3 (a) shows the geometry of the first lamella at dimensionless time $t = 2.6$, when the medication reaches for the first time the entrance of the micro-chamber. As time proceeds, the process of creation of the lamellae repeats itself, and a new pair of lamellae is produced at each period of forcing, i.e. a time unit, see figure 3 (b) at time $t = 3.6$. As the lamellae flow around the cylindrical obstacle they stretch against it and, eventually, they split into two streams of lamellae moving around the obstacle and inducing further stretching and folding therefore favoring homogenization of the mixture by molecular diffusion, see figure 3 (c) at time $t = 7.6$). As the two streams of lamellae reconnect after bypassing the obstacle, see figure 3 (d) at time $t = 11.6$, further stretching and folding is induced as the lamellae flow out through the exit micro-channel. As time further proceeds, the process continues robustly and the mixture slowly occupies the entire micro-chamber until it reaches regime conditions, as shown in figures 3 (e)-(g) at times $t = 19.6$, 39.6 and 199.6.

Figure 3 (h) presents a snapshot of the mixture inside our three-dimensional micro-mixer at dimensionless time $t = 199.6$. Since the concentration field is symmetric with respect to the mid-plane, only the top-half of the micro-mixer is shown in figure 3 (h). Lamellae of opposite concentrations are clearly recognizable in the mid-plane where they closely match the pattern of lamellae simulated using the two-dimensional model, compare with 3 (g). The lamellae within the micro-mixer are three-dimensional, as shown by the vertical slices in figure 3 (h), and they extend toward the top and bottom walls of the mixing micro-chamber where they are stretched by their interaction with the walls and, therefore, mixing is favored. Since the two fluids are mostly segregated in the symmetry plane at the entrance of the micro-chamber, and considering that the configuration of the lamellae in this plane is nearly identical to the configuration of the lamellae obtained using a two-dimensional model of the micro-mixer, we conclude that two-dimensional simulations are representative of the flow within the three-dimensional mixer and give accurate results. Therefore, we found more efficient and economical to study the dynamics of the lamellae and perform the characterization of the micro-mixer using the two-dimensional model. We will discuss the performance of the three-dimensional micro-mixer toward the end of this section.

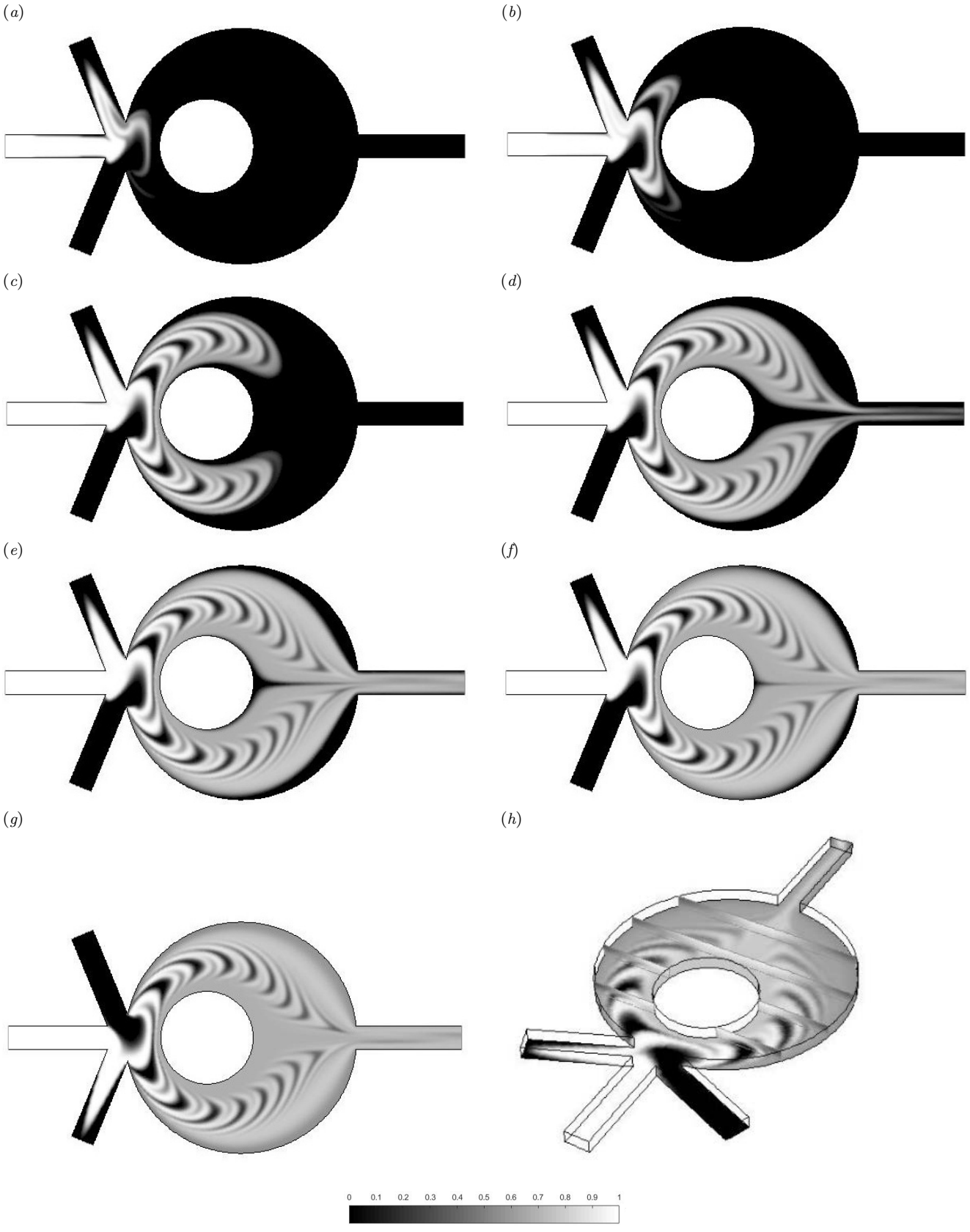

Fig. 3 Time-evolution of the two-dimensional concentration of the scalar field when $Re = 2$, $St = 0.8$ and $Pe = 10^4$: (a) $t = 2.6$, (b) $t = 3.6$, (c) $t = 7.6$, (d) $t = 11.6$, (e) $t = 19.6$, (f) $t = 39.6$, (g) $t = 199.6$. Panel h shows the concentration of the scalar field for the corresponding three-dimensional micro-mixer at $t = 199.6$. In particular, it shows the values of the concentration on the symmetry plane and several perpendicular planes.

In order to identify the range of operating conditions over which our micro-mixer is effective, we investigate, using the two dimensional model, how the mixing performance depends on the characteristic parameters: Reynolds, Strouhal and Péclet numbers. First, we study how the mixing performance depends on the Reynolds number by varying it, by changing the viscosity of the fluids, over two orders of magnitude, from 0.2 to 20. Figure 4 shows the time evolution of the mixing efficiency from dimensionless time $t = 0$ up to $t = 200$, when all cases are nearly at regime, for $Re = 0.2$, 1, 2, 5, 10, 15, and 20, Strouhal number $St = 0.8$ and Péclet number $Pe = 10^4$. For each Reynolds number considered, a black curve shows the time-evolution of the mixing performance, M, averaged over one period of forcing (see equation (4), where $Tot = 20$), measured at a cross-section of the exit micro-channel located at a distance l from the outlet. The shaded gray region that surrounds the black curve is actually the curve for the unaveraged mixing performance computed by removing the time average from equation (4). The gray curves show the level of oscillations that the concentration experiences near the outlet of the two-dimensional model. The frequency of these oscillations is twice the frequency of forcing, because the flow in opposition of phase in the side micro-channels generates a new set of lamellae at each half-period of forcing.

For all Reynolds numbers considered, from dimensionless time $t = 0$ to about $t = 10$, the mixing performance is zero (see figure 4) because the micro-mixer is initially full of carrier solution and, therefore, the mixture has not, as yet, reached the measurement cross-section near the end of the exit micro-channel, the concentration fields at these early times are shown in figures 3 (a)-(c) for the case $Re = 2$. As soon as the mixture reaches the measurement cross-section, the value of the mixing performance increases suddenly reaching 50% by about $t = 18$ in all cases but $Re = 0.2$ which is a little slower and reaches 50% by about $t = 20$. Also from $t = 20$, the time-evolution of the mixing performance for the different cases start to differ noticeably. By time $t = 40$ the mixing performance is greater than 80% for all cases but $Re = 0.2$ that barely reaches 70%. While most curves are monotonic or nearly so, the curves for the cases $Re = 5$ and 10 are noticeably different. In both cases the curves reach a maximum, about $M = 83.3\%$ at time $t = 37.5$ for the case $Re = 5$ and about $M = 88\%$ at time $t = 45$ for the case $Re = 10$, and then decrease substantially by the final time $t = 200$ where they reach the values of about $M = 72\%$ for the case $Re = 5$ and $M = 79.5\%$ for the case $Re = 10$, respectively. By time $t = 80$ all curves become monotonic and relax slowly toward their

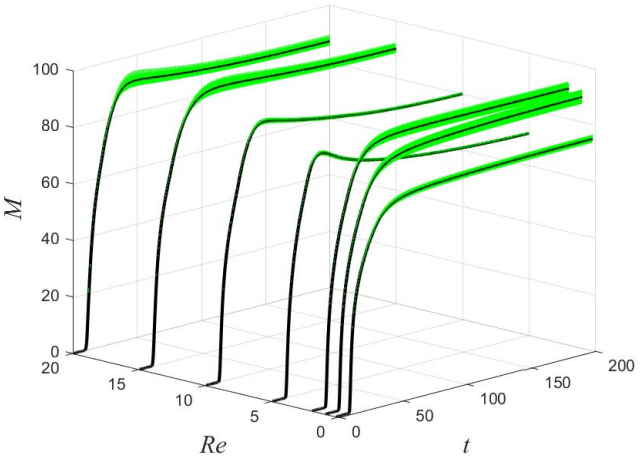

Fig. 4 Reynolds' number effects on the mixing performance of the micro-mixer when $St = 0.8$ and $Pe = 10^4$.

steady state value at around $t = 200$. By this time, at $Re = 0.2$, the lowest Reynolds number considered in this study, the mixing efficiency, M, is about 75%. The efficiency improves substantially as the Reynolds number increases from 0.2 to 1, where $M = 88.9\%$. A further improvement, although modest, is obtained by increasing the Reynolds number from 1 to 2 where the mixing efficiency reaches a peak value of 90.8%. At this point one would expect the mixing efficiency to keep increasing slowly as the Reynolds number increases. Surprisingly, this is not the case and, as the Reynolds number increases from 2 to 5, the mixing efficiency drops to its lowest value of about 71.5%. We will elaborate on the reasons for this drop farther in this section. As the Reynolds number further increases from 5 to 15 the mixing efficiency improves drastically and reaches a value of 90.2%, close to the peak value measured at $Re = 2$. A modest drop in efficiency can be observed as the Reynolds number reaches 20, where $M = 87.2\%$. The width of the gray regions, indicating the level of oscillation of the mixing performance, is also a source of surprise. One would expect the width of the gray region to decrease as mixing efficiency increases, in reality the trend is opposite. The value of the concentration of the mixture oscillates substantially less, about $\pm 0.5\%$, when the mixing performance is around 75%-80% than when it is around 90%, where the amplitude of the oscillations is about $\pm 3\%$. In the next paragraph we will also discuss this unexpected behavior.

Figure 5 shows the concentration of the scalar field when $Re = 0.2$ and $M = 75\%$ (a), $Re = 2$ and $M = 90.8\%$ (b), $Re = 5$ and $M = 71.5\%$ (c) and $Re = 15$ and $M = 90.2\%$ (d), at time $t = 199.6$ when $St = 0.8$ and $Pe = 10^4$. To understand the substantially differ-

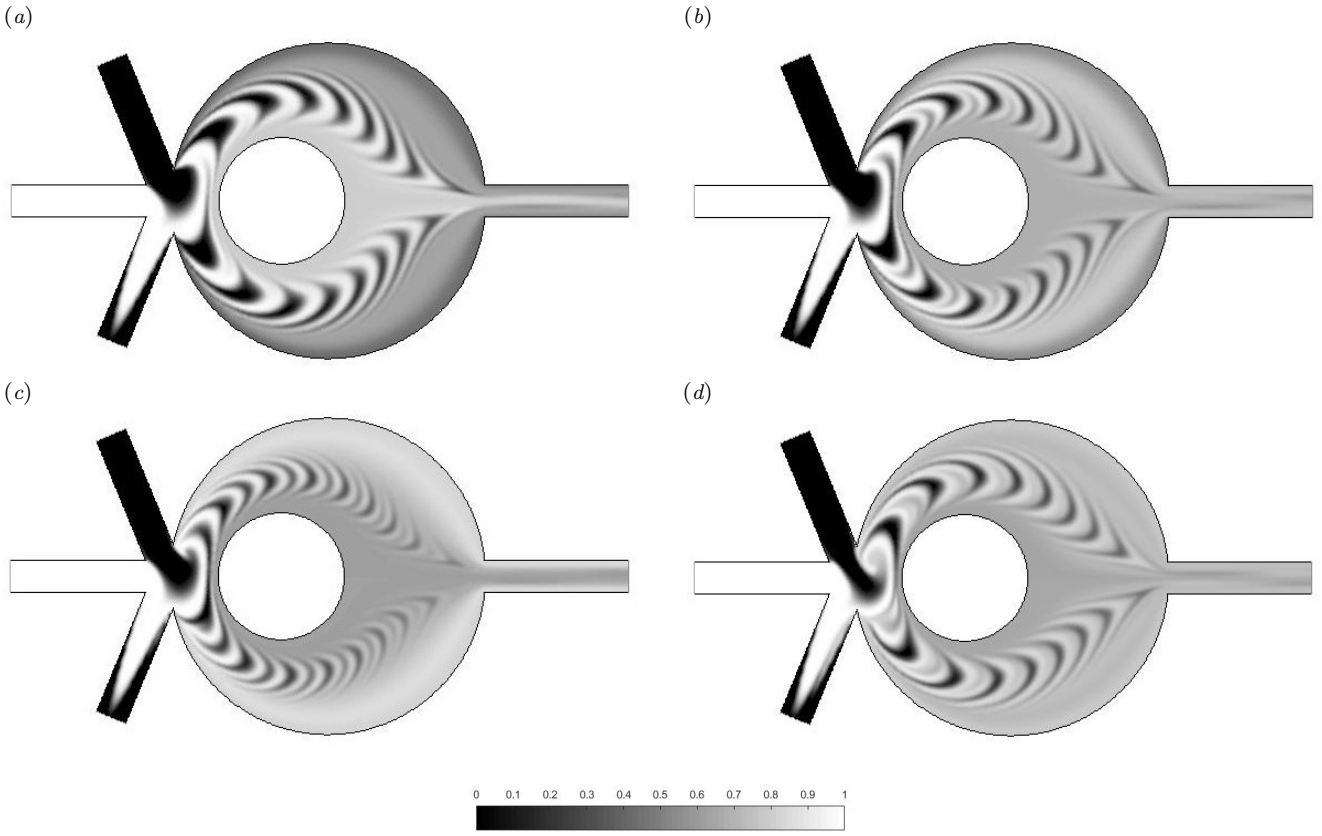

Fig. 5 Concentration of the scalar field at time $t = 199.6$ when $Re = 0.2$ (a), 2 (b), 5 (c) and 15 (b), $St = 0.8$ and $Pe = 10^4$.

ent mixing performance at different Reynolds numbers, it is important to note that the flow within the two-dimensional micro-chamber can be subdivided in three distinct regions: the region occupied by the lamellae and the two wall regions of almost uniform concentration surrounding the region occupied be the lamellae. Note that the uniform concentration in the wall regions is due to the combined action of shearing, that stretches the lamellae, and molecular diffusion that homogenize them. Intuitively, the flow in the region occupied by the lamellae of opposite concentration seems to be responsible for the overall mixing performance of our micro-mixer. After a careful analysis, however, it is evident that this is not the case, and that mixing within the two wall regions, around the obstacle and along the inner walls of the mixing micro-chamber, equally contribute to the mixing performance measured at the exit micro-channel. In fact, within the exit micro-channel the flow is laminar and five distinct layers of fluid can be recognized: two layers along the walls are fed by the flow along the walls of the micro-chamber, two layers are produced by the stretching and folding of the lamellae, and the central layer is the confluence of the flows (top and bottom) around the obstacle.

In the case $Re = 5$ (see figure 5 (c)), if one relies only on the appearance of the flow in the region occupied by the lamellae, where the lamellae are thin and almost perfectly alternated, one would come to the conclusion that this case produces the best mixing performance, a wrong conclusion indeed, since the mixing performance, at regime, is only about 71.5% (as shown by figure 4). The reason for such a poor performance is that the flows in the wall regions are well homogenized but the concentration of the medication (white fluid) is too high along the walls of the mixing chamber and too low around the obstacle, as shown in figure 5 (c) by the light and dark shades of gray of the fluid layers in the exit micro-channel. On the other hand, when $Re = 2$ (figure 5 (b)) or $Re = 15$ (figure 5 (d)), although there are differences in the dynamics of the formation of the lamellae and their structure, the mixing performance is nearly the same for both cases because the mixture in the wall regions is almost perfectly mixed. In these two cases, $Re = 2$ and 15, the lamellae are not as thin and uniformly distributed as in the case $Re = 5$ and this fact explains the larger fluctuations of the concentration values shown by the width of the gray regions surrounding the black curve, see figure 4.

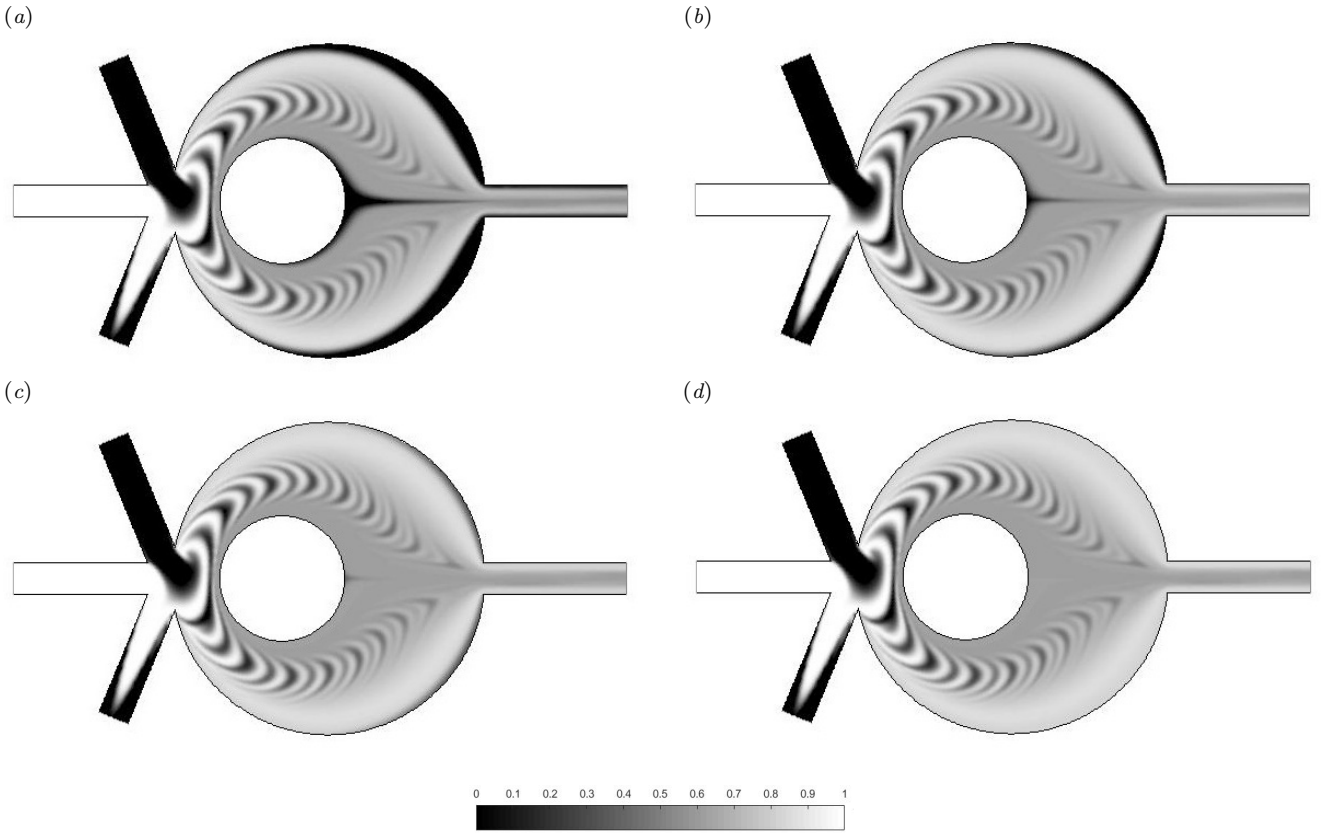

Fig. 6 Concentration of the scalar field at time $t = 20$ (a), 40 (b), 80 (c) and 200 (d) when $Re = 5$, $St = 0.8$ and $Pe = 10^4$.

Figure 6 sheds more light on the peculiar time evolution of the mixing performance of the two-dimensional model when $Re = 5$, $St = 0.8$ and $Pe = 10^4$. Figure 6 (a) presents a snapshot of the concentration field at $t = 20$ when the mixing performance is increasing quickly and the value is about $M = 58\%$. Note that by this time the mixture has not flushed the carrier solution completely out of the mixing micro-chamber and the carrier solution still occupies a minor area of the mixing chamber and the outer layers in the exit micro-channel (see black regions). By the time $t = 40$, when M is about 83.2%, the two-dimensional model has just passed its peak mixing performance and a snapshot of the concentration field at this time is shown in figure 6 (b). Note that by this time the mixture has filled completely the exit micro-channel, however, the mixture has not yet flushed the carrier solution completely out of the mixing micro-chamber. As time increases further, the mixing performance unexpectedly, starts decreasing and by time $t = 80$ reaches about 76.2% and keep decreasing reaching a nearly steady state value of about 71.5% at $t = 200$. A careful analysis shows that a subtle process is responsible for this behavior: the development of the wall flows around the circular obstacle and the outer walls of the mixing micro-chamber. As the mixture fills out the entire micro-chamber and flushes the carrier solution out, the tips of the lamellae are increasingly stretched by their interaction with of the obstacle and outer walls of the micro-chamber. As time increases, the flow around the obstacle becomes darker gray while the flow along the outer walls becomes lighter gray. It is this slow, almost imperceptible, change in concentration in the wall regions that it is responsible for the decrease in mixing performance of the two-dimensional model.

As a second step in characterizing the operating range of our micro-mixer, we investigate how its mixing performance depends on the Strouhal number. Figure 7 shows the time-evolution of the mixing efficiency of the two-dimensional model for $St = 0.4$, 0.6, 0.8, 1 and 1.2, Reynolds number $Re = 2$ and Péclet number $Pe = 10^4$. As before, for each Strouhal number considered, a black curve shows the time-evolution of the mixing performance, M, averaged over one period of forcing (see equation (4), where $Tot = 20$), and the shaded gray region that surrounds it shows the level of oscillations that the concentration experiences near the outlet of the two-dimensional model. We choose this range

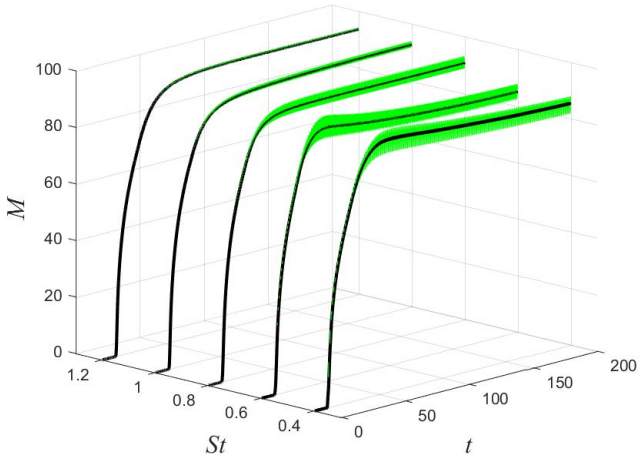

Fig. 7 Strouhal's number effects on the mixing performance of the micro-mixer when $Re = 2$ and $Pe = 10^4$.

of Strouhal numbers because for values below $St = 0.4$ the mixing efficiency of our micro-mixer becomes unattractive while for values above $St = 1.2$ the frequency of forcing becomes too high to be implemented in practical applications. Figure 7 shows that mixing efficiency increases monotonically as the Strouhal number increases, however, the trend is weakly nonlinear as the larger mixing improvement is obtained at around $St = 0.8$ where M is about 90.8%. On the other hand, as the Strouhal number increases above the value of 0.8, the increase in mixing efficiency weakens as perfect mixing ($M = 100\%$) is approached, we report a value of about 93.7% at $St = 1.2$. The width of the gray regions, indicating the level of oscillation of the mixing performance, provides further evidence that the homogeneity of the mixture increases as the Strouhal number increases. The width of the gray regions decreases from about $\pm$ 3% at $St = 0.4$ to almost zero at $St = 1.2$, indicating that the thickness of the lamellae produced by forcing are responsible for the oscillations of the value of concentration measured near the outlet. At $St = 1.2$ the lamellae are sufficiently thin that molecular diffusion almost perfectly homogenizes the mixture by the time it reaches the outlet of the micro-mixer.

Ideally, therefore, one would like to operate the micro-mixer at a Strouhal number as high as possible, in order to produce thinner and thinner lamellae of concentration so that molecular diffusion could complete the mixing process ($M = 100\%$) before the mixture exits the micro-mixer. However, implementing high Strouhal numbers operating conditions implies the generation of high frequencies of forcing, which are difficult to achieve with currently available micro-pumps. The results shown in figure 7 indicate, as the best compromise, to operate the micro-mixer at a Strouhal number of about 0.8 where the frequency of forcing is realistic and the fluctuations in concentration are acceptable.

To finish characterizing the design of our micro-mixer, we study the effect of the Péclet number on its mixing performance. We let the Péclet number vary between 10^3 and 10^5 because these are the typical values of many challenging mixing applications. For Péclet numbers below the lower bound, mixing starts to be strongly favored by molecular diffusivity, while for Péclet numbers above the upper bound, promoting mixing becomes extremely difficult. Figure 8 shows the time evolution of the mixing efficiency for $Pe = 10^3$, 10^4, and 10^5, Reynolds number $Re = 2$ and Strouhal number $St = 0.8$. As before, for each Péclet number considered, a black curve shows the time-evolution of the mixing performance, M, averaged over one period of forcing (see equation (4), where $Tot = 20$), and the shaded gray region that surrounds it shows the level of oscillations that the concentration experiences near the outlet of the two-dimensional model. The trend of the mixing performance, M, as expected, decreases weakly as the Péclet number increases, from about 92.9% at $Pe = 10^3$ to about 90.8% at $Pe = 10^5$. The results shown in figure 8 confirm the robustness of the design of our micro-mixer which has an excellent mixing performance ($M > 90\%$) even in conditions of weak diffusion ($Pe = 10^5$). As expected, the width of the gray regions shows that the homogeneity of the mixture increases as the Péclet number decreases. At $Pe = 10^3$, molecular diffusion is sufficiently strong to homogenize, within about $\pm$0.5%, the mixture produced by a forcing corresponding to a medium Strouhal number, $St = 0.8$.

Leveraging the insight obtained from the analysis of the mixing performance of the two-dimensional model, we can now discuss the performance of the three-dimensional micro-mixer. Figures 2 (a) and figure 2 (b), and figure 3 (g) and 3 (h) clearly show that the two-dimensional model captures accurately the dynamics of the concentration field in the mid-plane of the three-dimensional micro-mixer both in steady and unsteady flow conditions. Based on this observation, it is legitimate to expect the mixing performance of the two-dimensional model to be an accurate predictor of the mixing performance the three-dimensional micro-mixer. This is indeed the case if we measure the concentration of the mixture on a line lying across the mid-plane of the exit micro-channel, as for the two-dimensional model. However, if we measure the concentration of the mixture on a section of the exit micro-channel located in correspondence to the line in the two-dimensional model, the results change substantially and unexpectedly as shown in figure 9. This figure allows the comparison of

the time evolutions of the mixing performance for the steady ($Re = 2$ and $Pe = 10^4$) two-dimensional (dashed line) and three-dimensional (dot-dashed line) cases, and unsteady ($Re = 2$, $St = 0.8$ and $Pe = 10^4$) two-dimensional (dotted line) and three-dimensional (solid line) cases. The two pairs of curves depict some interesting but puzzling results. In the steady case, at final time $t = 200$, the three-dimensional micro-mixer performs 36.4% better than the two-dimensional model, while in the unsteady case, the three-dimensional micro-mixer performs 28.6% worse than the two-dimensional model. One should conclude that the flow, although symmetrical with respect to the mid-plane of the micro-mixer, is substantially three-dimensional and affects, for the better or the worse, the mixing performance measured near the end of the exit micro-channel. In particular, in the unsteady case, at final time $t = 200$, the mixing performance of the two-dimensional model is 90.8% while the performance of the three-dimensional micro-mixer is 69.3%. The reason for this somehow mediocre performance is to be found in the flow in the wall regions as for the two-dimensional case at $Re = 5$, $St = 0.8$ and $Pe = 10^4$ discussed above. Apparently, in the three-dimensional case, the flow in the wall regions (near the top and bottom of the mixing chamber, the side walls of the chamber and the cylindrical obstacle) strongly influences the mixing performance of the micro-mixer. The vertical slices in figure 3 (h) show that the black lamellae do not reach the top wall of the micro-chamber. Apparently, the black fluid injected at unsteady volume flow rate through the lateral micro-channels interacts with the steady flow of the white fluid by creating black lamellae enveloped by white fluid. In other words, the black fluid appears to be more segregated than the white fluid which surrounds it. This explains a higher concentration of medication (white fluid) near the top and bottom wall of the micro-chamber. On the other hand, the black lamellae appear to envelop the white lamellae toward the side walls of the micro-chamber producing a lower concentration of medication (a darker gray fluid) in these regions. As the mixture exits the micro-chamber, it forms an almost horizontally layered flow in the exit micro-channel, with darker gray fluid near the left and right walls and lighter gray fluid in the center, which is responsible for the mediocre mixing performance.

Finally, we address the geometrical scalability of our micro-mixer. Scalability is the most ambitious goal of an engineering design, often hard or impossible to obtain, as, for example, in the case of wing design. A scalable device works robustly and consistently at different length scales provided the same dimensionless specifications (e.g. Reynolds number, Strouhal number, Péclet

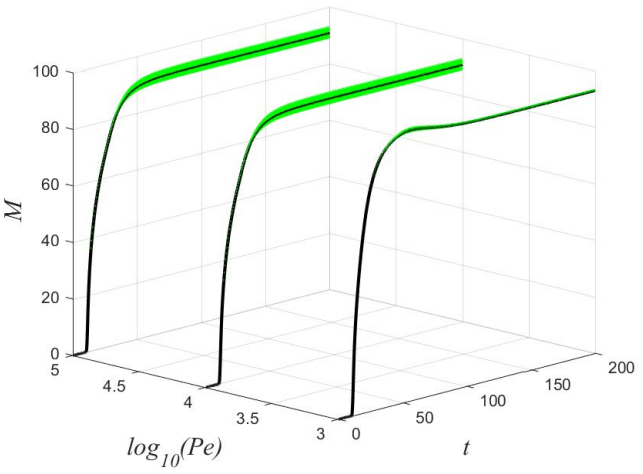

Fig. 8 Péclet's number effects on the mixing performance of the micro-mixer when $Re = 2$ and $St = 0.8$.

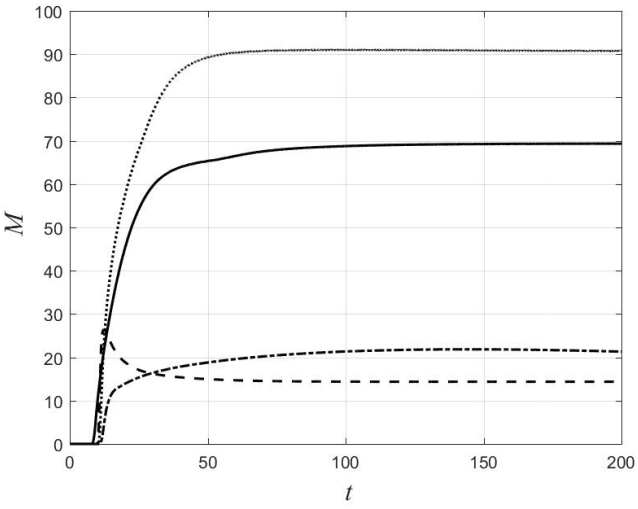

Fig. 9 Comparison of the time evolution of the mixing performance for the steady ($Re = 2$ and $Pe = 10^4$) two-dimensional (dashed line, figure 2 (a)) and three-dimensional (dot-dashed line, figure 2 (a)) cases and unsteady ($Re = 2$, $St = 0.8$ and $Pe = 10^4$) two-dimensional (dotted line, figure 3 (g)) and three-dimensional (solid line, figure 3 (h)) cases.

number, etc.) can be maintained constant. Based on the above results, we tested the geometrical scalability of the reference three-dimensional micro-mixer of dimensions $W_r = 200\mu m$, $R = 2.5W_r$, $r = W_r$, $l = 0.5W_r$, $L_{in} = 2W_r$, $L_{out} = 2.25W_r$, $C_c - C_o = 0.75W_r$, $\alpha = 67.5°$, volume flow rates $Q_{Mr} = 10^8\mu m^3/s$, $Q_{Cr} = Q_{Mr}/2$, $Q_{Or} = 4Q_{Mr} = 8Q_{Cr}$, and frequency of forcing $f_r = 40Hz$ when operating at $Re = 2$, $St = 0.8$ and $Pe = 10^4$. The total volume of the reference mixer is of $83.4 \times 10^6\mu m^3 = 1.0425 \times W_r^3$ and the time necessary to fill it with fluid is $0.56s$ or 22.4 periods of forcing. In order to reproduce the same operating conditions,

we scaled the geometric dimensions of our micro-mixer, the volume flow rates at the inlets and the frequency of forcing to maintain constant the values of Reynolds, Strouhal and Péclet numbers, respectively. Introducing a scaling factor S, the scaled geometry is obtained simply by multiplying the geometric dimensions of the reference micro-mixer by S, therefore, when $S < 1$ the micro-mixer is scaled down, while when $S > 1$ the micro-mixer is scaled up. It is easy to show that to maintain constant the values of Reynolds, Strouhal and Péclet numbers, the velocities at the inlets should be obtained from the reference velocities multiplying them by S^{-1} and the forcing frequency should be obtained from the reference frequency multiplying it by S^{-2}. In other words, the characteristic length scale is $W = S \times W_r$, the characteristic velocity is $V = V_r/S$ and the characteristic frequency is $f = f_r/S^2$, i.e. velocities and frequency must to be increased as the geometric dimensions are decreased and viceversa.

Figure 10 shows the relationship between scaling factor and frequency of forcing, the latter being the most critical and influential parameter of our active micro-mixer. The reference case corresponds to $S = 1$, of course. This figure gives insight about the difficulty of aggressively scaling down (i.e., $S < 1$) the reference micro-mixer because of the high frequencies required to operate it effectively. Comparing the concentration maps, we were able to verify, for three values of the scaling factor, $S = 0.5$, 1 and 10, the relationships obtained analytically and discussed above. Note that the value of the forcing frequency for the case $S = 0.1$ is the analytical value, i.e. $f = 4000Hz$. In this case, the required frequency of forcing becomes prohibitively high even for a numerical simulation. On the other hand, it is easy to scale up (i.e., $S > 1$) the reference micro-mixer because the required forcing frequency becomes smaller and smaller (e.g., $f = 0.4Hz$ for $S = 10$) as the micro-mixer's size becomes larger and larger.

Figure 11 provides an effective visual comparison between the geometries and mixing performance of three micro-mixers corresponding to $S = 0.5, 1$ and 10, when operating at $Re = 2$, $St = 0.8$ and $Pe = 10^4$. The dark-framed concentration fields indicate the actual size of the micro-mixers when compared to the size of a coin of 1 cent of euro, whose real diameter is $16250\mu m$. The unframed concentration fields for the cases $S = 0.5$ and 1 have been plotted to have the same size as the (dark-framed) concentration field for the case $S = 10$ to allow a precise comparison. In all three cases, the concentration fields appear to be nearly identical and, in fact, the mixing performance of the three micro-mixers is nearly the same.

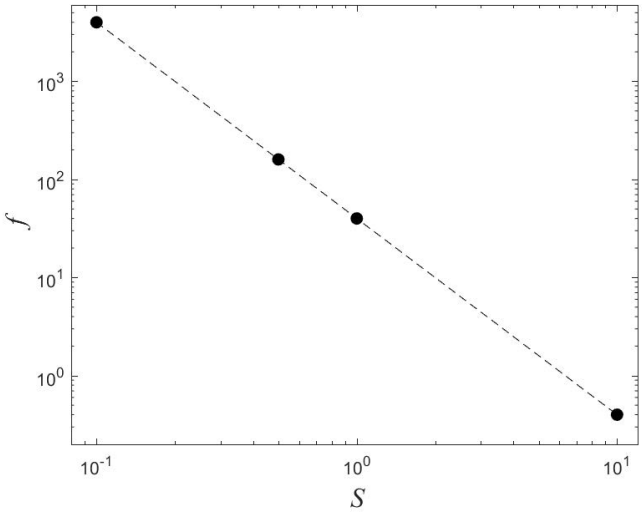

Fig. 10 Scaling factor, S, versus frequency of forcing, f.

4 Conclusions

We presented a novel, compact, geometrically scalable, active micro-mixer able to process volumes of fluid in the range of $10^{-6} \div 10^{-9}$ liters. The micro-mixer has been designed with a simple geometry to facilitate its manufacturing and assimilation in different LoC and other platforms, a sort of one-design-fits-all. The micro-mixer produces rapid mixing because of its active actuation system, that generates lamellae of opposite concentration, and its geometry, that favors the folding and stretching of these lamellae.

We studied numerically the mixing performance of our micro-mixer both in three- and two-dimensions by leveraging the fact that the flow within the micro-mixer is symmetric with respect to the mid-plane and the concentration field in the mid-plane is the less well mixed. To reduce computational time, we first optimized the design of our-micro-mixer and its mixing performance using the two-dimensions model. We characterized the mixing performance in terms of Reynolds, Strouhal and Péclet numbers in order to establish a practical range of operating conditions for our micro-mixer. The two-dimensional model has a mixing efficiency above 90% for a wide range of Strouhal and Péclet numbers, i.e. $St > 0.75$ and $Pe < 10^5$. Its performance, however, is not uniform in terms of Reynolds number due to the transition between two different mixing regimes at about $Re = 2$ and 15, respectively. However, the performance can be easily made uniform over the entire range of Reynolds numbers considered by operating the mixer at higher Strouhal numbers where it is needed.

Although, the time-evolution of the flow in the mid-plane of the three-dimensional micro-mixer is nearly

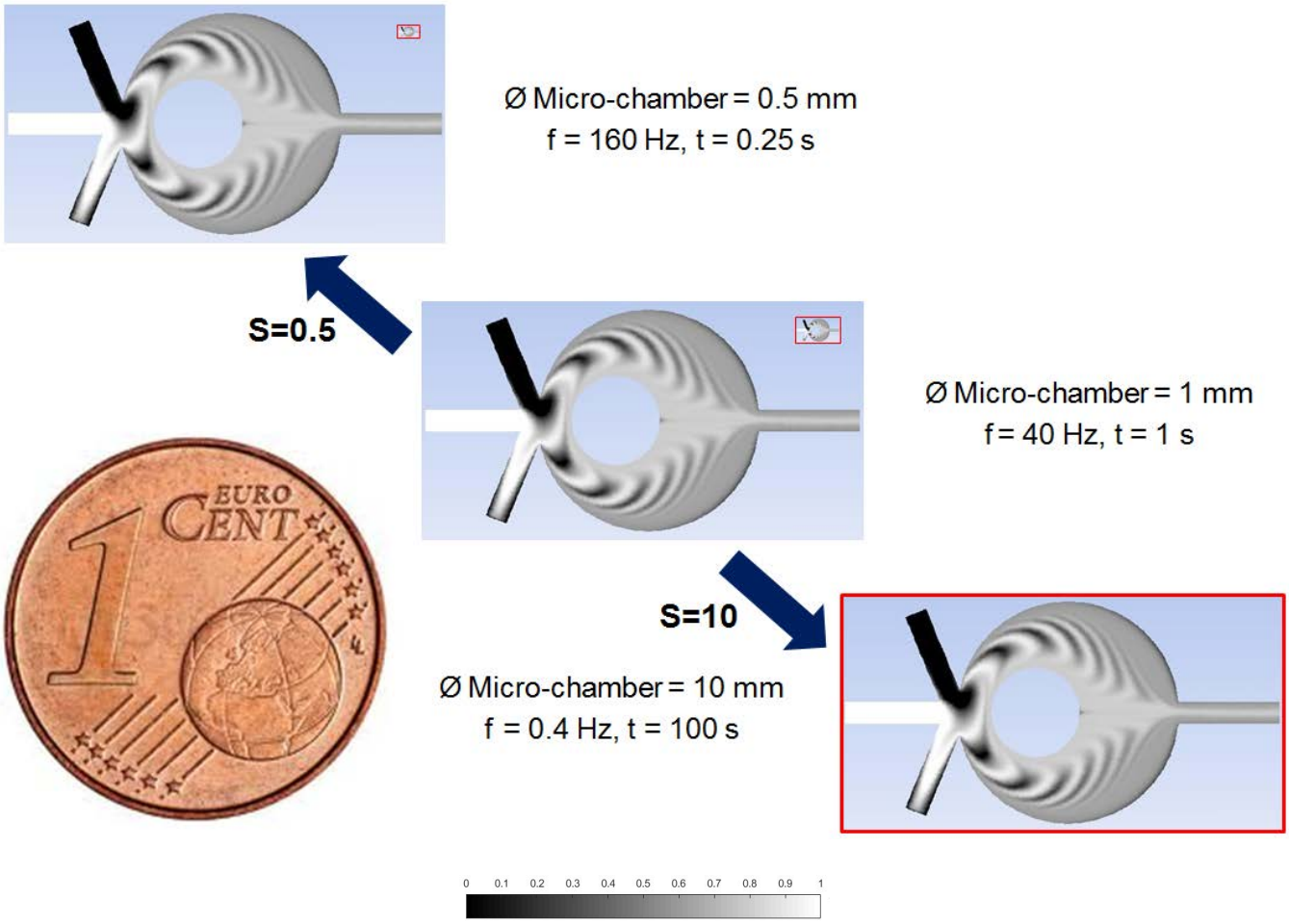

Fig. 11 Comparison between the geometries and mixing performance of three micro-mixers corresponding to the scaling factor $S = 0.5, 1$ and 10, when operating at $Re = 2$, $St = 0.8$ and $Pe = 10^4$. The dark-framed concentration fields indicate the actual size of the micro-mixers when compared to the size of a coin of 1 cent of euro, whose real diameter is $16250\mu m$. The mixing performance can be visually assessed by comparing the unframed concentration fields for the cases $S = 0.5$ and 1 with the dark-framed concentration field for the case $S = 10$

identical to the flow within the two-dimensional model, the relationship between the mixing performance of the two- and three-dimensional micro-mixers is not trivial and strongly depends on how and where the concentration of the mixture is measured. If we measure the concentration of the mixture on a line lying across the mid-plane of the exit micro-channel, as for the two-dimensional model, the agreement is excellent. However, if we measure the concentration of the mixture on a section of the exit micro-channel located in correspondence to the line in the two-dimensional model, the results change substantially and unexpectedly. For the reference case $Re = 2$, $St = 0.8$ and $Pe = 10^4$, the mixing performance of the two-dimensional micro-mixer is about 90.8%, while the performance of the three-dimensional micro-mixer is merely 69.3%. The reason for such a major difference in performance has to be found in the flows along the inner walls of the three-dimensional micro-mixer, in particular the top and bottom walls of the mixing chamber that account for more than 90% of the walls surface area. A careful analysis of the velocity and concentration fields for the three-dimensional micro-mixer shows that the interaction, at the entrance of the micro-chamber, between the steady stream of medication (white fluid) and the unsteady streams of carrier solution (black fluid) creates lamellae of opposite concentration, with the white lamellae enveloping the black lamellae toward the top and bottom of the mixing micro-chamber, and the black lamellae enveloping the white ones toward the sides of the micro-chamber. The geometrical structure of the lamellae reaches into the wall regions, where the lamellae are stretched, producing an almost homogeneous mixture of too high concentration (light gray) near the top and

bottom walls of the micro-chamber and a too low concentration (dark gray) near the side walls. Ultimately, the flows in the wall regions are mostly responsible for a stream of over- and under-diluted medication on the sides and in the center of the exit micro-channel, respectively, and, therefore for the mediocre performance of the three-dimensional micro-mixer. The discrepancy in performance between the two-dimensional model and three-dimensional micro-mixers shows that the results strongly depend on how and where the concentration of the mixture is measured and, therefore, the results obtained using a two-dimensional model cannot be trusted to predict the results of the corresponding three-dimensional micro-mixer. In our case, however, the performance of the three-dimensional micro-mixer can be easily improved by increasing the operating Strouhal number. A higher frequency of forcing, although more expensive to produce, will generate finer lamellae therefore mitigating the three-dimensional effects described above and improving significantly the mixing performance.

We showed that our three-dimensional micro-mixer is geometrically scalable. In other words, micro-mixers of different geometrical dimensions having the same nondimensional specifications produce nearly the same mixing performance. In order to reproduce the same operating conditions, we scaled the dimensions of our micro-mixer, the velocities at the inlets and the frequency of forcing to maintain constant the values of Reynolds, Strouhal and Péclet numbers, respectively. We believe that the successful scalability of our micro-mixer is due to the strong laminarity of the velocity vector field over the entire parameter space. The laminar flow is deformed by the oscillating lateral streams in nearly the same way at different geometrical dimension provided the micro-mixers operate at the same values of Reynolds, Strouhal and Péclet numbers. We observed that aggressive scaling down can be difficult because the frequency of forcing increases with the inverse of the scaling factor squared. On the other hand, scaling up is easier because the required frequency of forcing becomes lower and lower as the size of the micro-mixer become larger and larger.

In conclusion, the proposed micro-mixer can find applications on several platforms, operating in coordinations with other microfluidic devices, as in a LoC, or operating independently. Our micro-mixer can operate in series (or in cascade), i.e. the exit micro-channel of a micro-mixer can be connected to the entrance micro-channel of another (twin) micro-mixer in order obtain a mixture of the required concentration.

Acknowledgements One of the authors, S. F., thanks Dr. Chiara Corsini, Dr. Claudio Chiastra and Dr. Elena Bianchi for their kind guidance in developing the numerical model using ICEM and Ansys Fluent 14 (Ansys, Canonsburg, PA, USA) and their support in running the numerical simulations.

References

1. Burns MA, Johnson BN, Brahmasandra SN, Handique K, Webster JR, Krishnan M, Sammarco TS, Man PM, Jones D, Heldsinger D, Mastrangelo CH, Burke DT, An integrated nanoliter DNA analysis device, Science, 282, 484-487 (1998)
2. Mark D, Haeberle S, Roth G, von Stetten F, Zengerle R, Microfluidic lab-on-a-chip platforms: requirements, characteristics and applications, Chemical Society Reviews, 39, 1153-1182 (2010)
3. Whitesides G, Solving problems, Lab on a Chip, 10, 2317-2318 (2010)
4. Stahl M, Aslund BL, Rasmuson AC, Reaction crystallization kinetics of benzoic acid, AlChE Journal, 47, 1544-1560 (2001)
5. Yun K-S, Yoon E, Microfluidic components and bioreactors for miniaturized bio-chip applications, Biotechnology and Bioprocess Engineering, 9, 86-92 (2004)
6. Nie Z, Xu S, Seo M, Lewis PC, Kumacheva E, Polymer particles with various shapes and morphologies produced in continuous microfluidic reactors, Journal of the American Chemical Society, 127, 8058-8063 (2005)
7. Pennemann H, Hessel V, Kost H-J, Lwe H, de Bellefon C, Investigations on pulse broadening for catalyst screening in gas/liquid systems, AlChE Journal, 50, 1814-1823 (2004)
8. Hessel V, Lwe H, Organic synthesis with microstructured reactors, Chemical Engineering & Technology, 28, 267-284 (2005)
9. Daito N, Aoki N, Yoshida J-I, Mae K, Selective condensation reaction of phenols and hydroxybenzyl alcohol using micromixers based on collision of fluid segments, Industrial and Engineering Chemistry Research, 45, 4954-4961 (2006)
10. Burke BJ, Regnier FE, Stopped-flow enzyme assays on a chip using a microfabricated mixer, Analytical Chemistry, 75, 1786-1791 (2003)
11. Sundberg SA, High-throughput and ultra-high-throughput screening: solution- and cell-based approaches, Current Opinion in Biotechnology, 11, 47-53 (2000)
12. Dunn DA, Feygin I, Challenges and solutions to ultra-high-throughput screening assay miniaturization: submicroliter fluid handling, Drug Discovery Today, 5, S84-S91 (2000)
13. Battersby, BJ, Trau M, Novel miniaturized systems in high-throughput screening, Trends in Biotechnology, 20, 167-173 (2002)
14. Dittrich PS, Jahnz M, Schwille P, A new embedded process for compartimentalized cell-free protein expression and on-line detection in microfluidic devices, ChemBioChem, 6, 811-814 (2005)
15. Hsu C-H, Folch A, Spatio-temporally-complex concentration profiles using a tunable chaotic micromixer, Applied Physics Letters, 89, Article number 144102 (2006)
16. Lu H, Schmidt MA, Jensen KF, A microfluidic electroporation device for cell lysis, Lab on a Chip, 5, 23-29 (2005)
17. Chun H, Kim HC, Chung TD, Ultrafast active mixer using polyelectrolytic ion extractor, Lab on a Chip Miniaturisation for Chemistry and Biology, 8, 764-771 (2008)

18. Chang Y-H, Lee G-B, Huang F-C, Chen Y-Y, Lin J-L, Integrated polymerase chain reaction chips utilizing digital microfluidics, Biomedical Microdevices, 8, 215-225 (2006)
19. Min J, Kim JH, Kim S, Microfluidic device for bio analytical systems, Biotechnology and Bioprocess Engineering, 9, 100-106 (2004)
20. Roder H, Wuthrich K, Protein folding kinetics by combined use of rapid mixing techniques and NMR observation, Proteins: Structure, Function and Genetics, 1, 34-42 (1986)
21. Lipman EA, Schuler B, Bakajin O, Eaton WA, Single-molecule measurement of protein folding kinetics, Science, 301, 1233-1235 (2003)
22. Nguyen N-T, Wu Z, Micromixers a review, Journal of Micromechanics and Microengineering, 15, R1-R16 (2005)
23. Yang J-T, Lin K-W, Mixing and separation of two-fluid flow in a micro planar serpentine channel, Journal of Micromechanics and Microengineering, 16, 2439-2448 (2006)
24. Ravi Kumar DV, Prasad BLV, Kulkarni AA, Segmented flow synthesis of Ag nanoparticles in spiral microreactor: role of continuous and dispersed phase, Chemical Engineering Journal, 192, 357-368 (2012)
25. Hardt S, Pennemann H, Schönfeld F, Theoretical and experimental characterization of a low-Reynolds number split-and-recombine mixer, Microfluid Nanofluid, 2, 237-248 (2006)
26. Aref H, Stirring by chaotic advection, Journal of Fluid Mechanics, 143, 1-21 (1984)
27. Johnson TJ, Ross D, Locascio LE, Rapid microfluidic mixing, Analytical Chemistry, 74, 45-51 (2002)
28. Stroock AD, Dertinger SKW, Ajdari A, Mezi I, Stone HA, Whitesides GM, Chaotic mixer for microchannels, Science, 295, 647-651 (2002)
29. Ottino JM, Wiggins S, Designing optimal micromixers, Science, 305, 485-486 (2004)
30. Kim DS, Lee SW, Kwon TH, Lee SS, A barrier embedded chaotic micromixer, Journal of Micromechanics and Microengineering, 14, 798-805 (2004)
31. Garofalo F, Adrover A, Cerbelli S, Giona M, Spectral characterization of static mixers. The S-shaped micromixer as a case study, AICHE Journal, 56, 318-335 (2010).
32. Glasgow I, Aubry N, Enhancement of microfluidic mixing using time pulsing, Lab on a Chip Miniaturisation for Chemistry and Biology, 3, 114-120 (2003)
33. Glasgow I, Lieber S, Aubry N, Parameters influencing pulsed flow mixing in microchannels, Analytical Chemistry, 76, 4825-4832 (2004)
34. Mao H, Yang T, Cremer PS, A microfluidic device with a linear temperature gradient for parallel and combinatorial measurements, Journal of the American Chemical Society, 124, 4432-4435 (2002)
35. El Moctar AO, Aubry N, Batton J, Electro-hydrodynamic micro-fluidic mixer, Lab on a Chip, 3, 273-280 (2003)
36. Deval J, Tabeling P, Ho C-M, A dielectrophoretic chaotic mixer, Proceedings of the IEEE Micro Electro Mechanical Systems (MEMS), 36-39 (2002)
37. Oddy MH, Santiago JG, Mikkelsen JC, Electrokinetic instability micromixing, Analytical Chemistry, 73, 5822-5832 (2001)
38. Bau HH, Zhong J, Yi M, A minute magneto hydro dynamic (MHD) mixer, Sensors and Actuators, B: Chemical, 79, 207-215 (2001)
39. Tseng W-K, Lin J-L, Sung W-C, Chen S-H, Lee GB, Active micromixers using surface acoustic waves on Y-cut 128 LiNbO3, Journal of Micromechanics and Microengineering, 16, 539-548 (2006)
40. Cubaud T, Mason TG, High-viscosity fluid threads in weakly diffusive microfluidic systems, New Journal of Physics, 11, Article number 075029 (2009)
41. Müller SD, Mezić I, Walther JH, Koumoutsakos P, Transverse momentum micromixer optimization with evolution strategies, Computers and Fluids, 33, 521-531 (2004)
42. Bottausci F, Cardonne C, Meinhart C, Mezić I, An ultrashort mixing length micromixer: The shear superposition micromixer, Lab Chip, 7, 396398 (2007)
43. Sun C-L, Sie J-Y, Active mixing in diverging microchannels, Microfluidics and Nanofluidics, 8, 485-495 (2010)
44. Ottino JM, The kinematics of mixing: stretching, chaos, and transport, Cambridge University Press, New York (1989)
45. Aref H, El Naschie MS, Chaos Applied to Fluid Mixing, Pergamon, New York (1995)
46. Alvarez MM, Muzzio FJ, Cerbelli S, Adrover A, Giona M, Self-similar spatiotemporal structure of intermaterial boundaries in chaotic flows, Phys. Rev. Lett., 81, 3395-3398, (1998)
47. Zalc JM, Muzzio FJ, Parallelcompetitive reactions in a two-dimensional chaotic flow, Chem. Engng Sci., 54, 10531069 (1999)
48. Aref H, The development of chaotic advection, Phys. Fluids, 14, 13151325 (2002)
49. Szalai ES, Kukura J, Arratia PE, Muzzio FJ, Effect of hydrodynamics on reactive mixing in laminar flows, Am. Inst. Chem. Eng. J., 49, 168179 (2003)
50. Gleeson JP, Transient micromixing: examples of laminar and chaotic stirring, Phys. Fluids, 17, 100614 (2005)
51. Gouillart E, Thiffeault J-L, Finn MD, Topological mixing with ghost rods, Phys. Rev. E, 73, 036311 (2006)
52. Phelps JH, Tucker CL, Lagrangian particle calculations of distributive mixing: limitations and applications, Chem. Engng Sci., 61, 68266836 (2006)
53. Sturman R, Ottino JM, Wiggins S, The Mathematical Foundations of Mixing: The Linked Twist Map as a Paradigm in Applications: Micro to Macro, Fluids to Solids, Cambridge University Press (2006)
54. Vikhansky A, Cox SM, Conditional moment closure for chemical reactions in laminar chaotic flows, Am. Inst. Chem. Eng. J., 53, 1927 (2007)
55. Cortelezzi L, Mezić I (eds), Analysis and control of mixing with an application to micro and macro flow processes, CISM Courses and Lectures 510, Springer Wien NewYork (2009)
56. Gubanov O, Cortelezzi L, Sensitivity of mixing optimization to the geometry of the initial scalar field, Analysis and control of mixing with an application to micro and macro flow processes, CISM Courses and Lectures 510, 369405, Springer Wien NewYork (2009)
57. Cortelezzi L, Adrover A, Giona M, Feasibility, efficiency and transportability of short-horizon optimal mixing protocols, J. Fluid Mech., 597, 199-231 (2008)
58. Gubanov O, Cortelezzi L, Towards the design of an optimal mixer, J. Fluid Mech., 651, 27-53 (2010)
59. Gubanov O, Cortelezzi L, On the cost efficiency of mixing optimization, J. Fluid Mech., 692, 112-136 (2011)
60. Ismagilov RF, Stroock AD, Kenis PJA, Whitesides G, Stone HA, Experimental and theoretical scaling laws for transverse diffusive broadening in two-phase laminar flows in microchannels, Appl. Phys. Let., 76, 2376-2378 (2000).

61. Patankar SV, Numerical heat transfer and fluid flow, Hemisphere Publishing/Taylor & Frances (1980)